International Journal of Chemistry, Mathematics and Physics (IJCMP)
[Vol-6, Issue-4, Jul-Aug, 2022]
https://dx.doi.org/10.22161/ijcmp.6.4.2
ISSN: 2456-866X

A Numerical Simulation of Soret-Dufour effect on Unsteady MHD Casson Fluid Flow past a vertical plate with Hall current and viscous dissipation

A.K. Shukla[1], Yogendra Kumar Dwivedi[2], Mohammad Suleman Quraishi[3]

[1]Department of Mathematics RSKD PG College, U.P., India.
[2]Department of Mathematics RSKD PG College, U.P., India.
[3]Department of Applied Sciences, Jahangirabad Institute of Technology, U.P., India
Corresponding Author: [1]ashishshukla1987@gmail.com

Received: 21 Jul 2022; Received in revised form: 05 Aug 2022; Accepted: 10 Aug 2022; Available online: 15 Aug2022

Abstract**—** *The Casson fluid model, which is very significant in the biomechanics and polymer processing industries, is another term used to describe non-Newtonian fluid behavior. This study of Casson fluid model on unsteady MHD Casson fluid flow with Soret-Dufour effect past a vertical plate embedded in porous medium in the presence of radiation with heat generation/absorption and viscous dissipation is presented in this research article as a numerical investigation of non Newtonian Casson fluid with applied effects. Regulating partial differential equations have been used to explain the mathematical model of the flow field. The Crank-Nicolson implicit finite difference approach has been used to numerically solve non-dimensionalized flow field governing equations. Concentration, temperature, and velocity profile effects of non-dimensional factors have been investigated using tables and graphs as aids. Tables have also been used to observe fluctuations in factors like skin friction, the Nusselt number, and the Sherwood number in relation to other parameters.*

Keywords**— *Casson Fluid, Magnetohydrodynamics, Order of chemical reaction, Soret and Dufour effects Viscous dissipation.***

I. INTRODUCTION

Shear stress and shear rate have a non-linear relationship that non-Newtonian fluid can decipher. Worldwide, non-Newtonian solutions are employed in the pharmaceutical and chemical industries as well. Examples include oils, deodorizers, chemicals, syrups, thick drinks, cleansers, and the production of many different colours. In place of ketchup, custard, tooth paste, wheat, paint, blood, and shampoo, there are still a variety of polymer liquids and salt explanations that aren't Newtonian fluids. Shear and shear tension are longitudinally correlated in Newtonian fluid. Newtonian fluids such as blood, shampoo, soap, certain oils, jellies, paints, and other different production & further technical needs cannot be represented. Numerous researchers, programmers, and scientists have studied various uses. Non-Newtonian fluids are much more difficult to investigate than Newtonian fluids, nevertheless. Direct evaluation of non-Newtonian fluid properties using Navier-Stokes equations is not possible. There are several dynamic behaviors of fluid models that have drawn the attention of academics, including power law, Bingham plastic, Brinkman type, Oldroyd-B, Maxwell, Walter-B, and Jeffrey. The Casson fluid model is a non-Newtonian fluid evolutional paradigm. Casson developed the Casson fluid to forecast the flow behaviors of the pigment-oil solution. Non-Newtonian fluids are widely used in engineering fields and other industries, and their applications are rather obvious. Numerous research on Non-Newtonian fluid flow applications have been conducted in the presence of various effects for many years, which has attracted the attention of

many mathematicians. Casson fluid, which exhibits elasticity in nature and is one of the non-Newtonian fluid kinds, includes things like honey, jelly, tomato sauce, and others. Casson fluid, which exhibits elasticity in nature and is one of the non-Newtonian fluid kinds, includes things like honey, jelly, tomato sauce, and others. Casson fluid can also be used to treat human blood. Liaquat Ali Lund et al.[1] is investigated the magnetohydrodynamic (MHD) flow of Casson nanofluid with thermal radiation over an unsteady shrinking surface. Shahanaz Parvin et al.[2] are discussed effects of the mixed convection parameter, concentration buoyancy ratio parameter, Soret–Dufour parameters, and shrinking parameter in MHD Casson fluid flow past shrinking sheet. Lahmar et al.[3] studied heat transfer of squeezing unsteady nanofluid flow under the effects of an inclined magnetic field and variable thermal conductivity. Mohamed R.Eid et al. [4] investigated numerically for Carreau nanofluid flow over a convectively heated nonlinear stretching surface with chemically reactive species. Hammad Alotaibi et al.[5] introduced the effect of heat absorption (generation) and suction (injection) on magnetohydrodynamic (MHD) boundary-layer flow of Casson nanofluid (CNF) via a non-linear stretching surface with the viscous dissipation in two dimensions. Asogwa and Ibe [6] investigated numerical approach of MHD Casson fluid flow over a permeable stretching sheet with heat and mass transfer taking into cognizance the various parameters present. Renu et al.[7] assessed the effect of the inclined outer velocity on heat and flow transportation in boundary layer Casson fluid over a stretching sheet. Ramudu et al. [8] highlighted the impact of magnetohydrodynamic Casson fluid flow across a convective surface with cross diffusion, chemical reaction, non-linear radiative heat. Recently Mahabaleshwar et al.[9] discussed the important roles of SWCNTs and MWCNTs under the effect of magnetohydrodynamics nanofluids flow past over the stretching/shrinking sheet under the repercussions of thermal radiation and Newtonian heating. Ram Prakash Sharma et al. [10] reports MHD Non-Newtonian Fluid Flow past a Stretching Sheet under the Influence of Non-linear Radiation and Viscous Dissipation. Naveed Akbar et al.[11] investigated Numerical Solution of Casson Fluid Flow under Viscous Dissipation and Radiation Phenomenon. Elham Alali et al. [12] studied MHD dissipative Casson nanofluid liquid film flow due to an unsteady stretching sheet with radiation influence and slip velocity phenomenon. T. M. Ajayi et al. [13] have studied Viscous Dissipation Effects on the Motion of Casson Fluid over an Upper Horizontal Thermally Stratified Melting Surface of a Paraboloid of Revolution: Boundary Layer Analysis. N. Pandya and A. K. Shukla [14] have analyzed Effects of Thermophoresis, Dufour, Hall and Radiation on an Unsteady MHD flow past an Inclined Plate with Viscous Dissipation. Mallikarjuna B, Ramprasad S and Chakravarthy YSK [15] Multiple slip and inspiration effects on hydromagnetic Casson fluid in a channel with stretchable walls. Bukhari Z, Ali A, Abbas Z, et al.[16] The pulsatile flow of thermally developed non-Newtonian Casson fluid in a channel with constricted walls. Divya BB, Manjunatha G, Rajashekhar C, et al.[17] Analysis of temperature dependent properties of a peristaltic MHD flow in a non-uniform channel: a Casson fluid model. Ahmad Sheikh N, Ling Chuan Ching D, Abdeljawad T, et al. [18] A fractal-fractional model for the MHD flow of Casson fluid in a channel. Haroon Ur Rasheed, Saeed Islam, Zeeshan, Waris Khan, Jahangir Khan and Tariq Abbas [19], Numerical modeling of unsteady MHD flow of Casson fluid in a vertical surface with chemical reaction and Hall current.

Our goal is to shed light on the impact of a vertical porous plate with Soret-Dufour, radiation, heat generation/absorption source/sink, and higher-order chemical reaction in this inquiry. With the aid of tables and figures, the impact of different physical parameters on velocity, temperature, and concentration profiles is explained. On the other hand, tables are used to discuss crucial physical parameters like shearing stress, the Nusselt number, and the Sherwood number.

II. MATHEMATICAL MODELING

The unsteady MHD viscous, incompressible electrically conducting fluid's casson flow past an impulsively begun, infinitely inclined, porous plate with changeable temperature and mass dispersion has been taken into consideration. The plate is placed in a porous material and is vertical. The x-axis is considered perpendicular to the plate, and the y-axis parallel to it. Additionally, it is first believed that the radiation heat flux in the x-direction is much smaller than that in the y-direction. The fluid's temperature and concentration are the same for the plate. The plate's temperature and concentration fall exponentially as a result of the impulsive motion along the x-axis against the gravitational field with constant velocity u_0 at time t. Since the induced magnetic field is very small and the transversely applied magnetic field's magnetic Reynolds number is also very small, it can be regarded as inconsequential. Cowling [21], the flow variables are just functions of y and t since the x-direction is infinite. For this problem with an unstable flow

field, the governing partial differential equations are given by:

Continuity equation:

$$\frac{\partial \bar{v}}{\partial \bar{y}} = 0 \quad \Rightarrow \quad \bar{v} = -v_0(\,constant\,) \tag{1}$$

2.1 Momentum equation:

$$\frac{\partial \bar{u}}{\partial \bar{t}} + \bar{v}\frac{\partial \bar{u}}{\partial \bar{y}} = \nu\left(1+\frac{1}{\beta}\right)\frac{\partial^2 \bar{u}}{\partial \bar{y}^2} + g\,\beta_t(\bar{T}-\bar{T}_\infty) + g\,\beta_c(\bar{C}-\bar{C}_\infty) - \frac{\sigma {B_0}^2 \sin^2\eta}{(1+m^2)}\bar{u} - \frac{\mu \bar{u}}{\rho \bar{K}} \tag{2}$$

2.2 Energy equation:

$$\rho_\infty C_p\left(\frac{\partial \bar{T}}{\partial \bar{t}} + \bar{v}\frac{\partial \bar{T}}{\partial \bar{y}}\right) = k\frac{\partial^2 \bar{T}}{\partial \bar{y}^2} - \frac{\partial q_r}{\partial \bar{y}} + \frac{\rho D_m K_T}{c_s}\frac{\partial^2 \bar{C}}{\partial \bar{y}^2} + \mu\left(\frac{\partial \bar{u}}{\partial \bar{y}}\right)^2 - \bar{Q}_0\left(\bar{T}-\bar{T}_\infty\right) \tag{3}$$

$$\frac{\partial \bar{C}}{\partial \bar{t}} + \bar{v}\frac{\partial \bar{C}}{\partial \bar{y}} = D\frac{\partial^2 \bar{C}}{\partial \bar{y}^2} + \frac{D_m K_T}{T_m}\frac{\partial^2 \bar{T}}{\partial \bar{y}^2} - k_r\left(\bar{C}-\bar{C}_\infty\right)^n \tag{4}$$

$k_r\left(\bar{C}-\bar{C}_\infty\right)^n$	terms in mass equation for higher order chemical reaction
n	order of chemical reaction
k_r	chemical reaction constant
$\bar{C}$	concentration
$\bar{T}$	temperature
$\bar{T}_\infty$	temperature of free stream
$\bar{C}_\infty$	concentration of free stream
β	Casson parameter
βc	coefficient of volume expansion for mass transfer
β_t	volumetric coefficient of thermal expansion
T_m	mean fluid temperature
q_r	radiative heat along y ∗ -axis
$\bar{Q}_0$	Coefficient of heat source/sink
ν	kinematic viscosity
$\bar{K}$	coefficient of permeability of porous medium
D_m	molecular diffusivity
k	thermal conductivity of fluid

c_p	specific heat at constant pressure
μ	viscosity
ρ	fluid density
σ	electrical conductivity
g	acceleration due to gravity
K_T	thermal diffusion ratio
m	Hall current parameter

In Equation(4); $k_r\left(\overline{C}-\overline{C}_\infty\right)^n$ has come on account of n[th] order chemical reaction.

The boundary conditions for this model are assumed as:

$$\left.\begin{array}{llll} \bar{t}\le 0; & \bar{u}=0, \quad v_0=-v_0 \qquad \overline{T}=\overline{T}_\infty, \quad \overline{C}=\overline{C}_\infty & & \forall\,\bar{y} \\ \bar{t}>0; & \bar{u}=u_0, \quad \overline{T}=\overline{T}_\infty+(\overline{T}_w-\overline{T}_\infty)e^{-At}, \quad \overline{C}=\overline{C}_\infty+(\overline{C}_w-\overline{C}_\infty)e^{-At} & & at\ \bar{y}=0 \\ & \bar{u}\to 0, \qquad \overline{T}\to\overline{T}_\infty, \qquad \overline{C}\to\overline{C}_\infty & as & \bar{y}\to\infty \end{array}\right\} \tag{5}$$

Where $A=\dfrac{v_0^{\,2}}{\nu}$

Roseland explained the term radiative heat flux approximately as

$$q_r=-\frac{4\sigma_{st}}{3a_m}\frac{\partial\overline{T}^{\,4}}{\partial\,\bar{y}^4} \tag{6}$$

Here Stefan Boltzmann constant and absorption coefficient are σ_{st} and a_m respectively.

In this case temperature differences are very-very small within flow, such that $\overline{T}^{\,4}$ can be expressed linearly with temperature. It is realized by expanding in a Taylor series about T_∞' and neglecting higher order terms, so

$$\overline{T}^{\,4}\cong 4\overline{T}_\infty^{\,3}\overline{T}-3\overline{T}_\infty^{\,4} \tag{7}$$

With the help of equations (6) and (7), we write the equation (3) in this way

$$\left.\begin{array}{l} \rho_\infty C_p\left(\dfrac{\partial\overline{T}}{\partial\bar{t}}+\bar{v}\dfrac{\partial\overline{T}}{\partial\,\bar{y}}\right)=k\dfrac{\partial^2\overline{T}}{\partial\,\bar{y}^2}+\dfrac{16\overline{T}_\infty^{\,3}\sigma_{st}}{3a_m}\dfrac{\partial^2\overline{T}}{\partial\,\bar{y}^2}+\dfrac{\rho D_m K_T}{c_s}\dfrac{\partial^2\overline{C}}{\partial\,\bar{y}^2} \\ +\mu\left(\dfrac{\partial\bar{u}}{\partial\,\bar{y}}\right)^2-\overline{Q}_0\left(\overline{T}-\overline{T}_\infty\right) \end{array}\right\} \tag{8}$$

Let us introduce the following dimensionless quantities

$$\left.\begin{aligned}
&u=\frac{\bar{u}}{u_0},t=\frac{\bar{t}{v_0}^2}{\nu},y=\frac{\bar{y}v_0}{\nu},\theta=\frac{\bar{T}-\bar{T}_\infty}{\bar{T}_w-\bar{T}_\infty},C=\frac{\bar{C}-\bar{C}_\infty}{\bar{C}_w-\bar{C}_\infty},\\
&G_m=\frac{\nu g\beta_c(\bar{C}_w-\bar{C}_\infty)}{u_0{v_0}^2},G_r=\frac{\nu\, g\beta_t(\bar{T}_w-\bar{T}_\infty)}{u_0{v_0}^2},K=\frac{{v_0}^2}{\nu^2}\bar{K},\\
&S_c=\frac{\nu}{D},P_r=\frac{\mu C_p}{k},R=\frac{4\sigma\bar{T}_\infty^{\,3}}{k_m\,k},S_r=\frac{D_mK_T(\bar{T}_w-\bar{T}_\infty)}{T_m\nu(\bar{C}_w-\bar{C}_\infty)}\\
&Q=\frac{Q_0\nu}{\rho c_p{v_0}^2},D_u=\frac{D_mK_T(\bar{C}_w-\bar{C}_\infty)}{c_sc_p\nu(\bar{T}_w-\bar{T}_\infty)},K_r=\frac{k_r\,\nu}{{v_0}^2},A=\frac{{v_0}^2}{\nu}\\
&Ec=\frac{{v_0}^2}{c_p(\bar{T}_w-\bar{T}_\infty)},M_1=\frac{\sigma{B_0}^2\nu\sin^2\eta}{(1+m^2){v_0}^2},n=1
\end{aligned}\right\} \quad (9)$$

Using substitutions of Equation 9, we get non-dimensional form of partial differential Equations 2, 8 and 4 respectively

$$\frac{\partial u}{\partial t}-\frac{\partial u}{\partial y}=\left(1+\frac{1}{\beta}\right)\frac{\partial^2 u}{\partial y^2}+G_r\theta+G_mC-\left(M_1+\frac{1}{K}\right)u \quad (10)$$

$$\frac{\partial\theta}{\partial t}-\frac{\partial\theta}{\partial y}=\frac{1}{P_r}\left(1+\frac{4R}{3}\right)\frac{\partial^2\theta}{\partial y^2}+D_u\frac{\partial^2C}{\partial y^2}+E_c\left(\frac{\partial u}{\partial y}\right)^2-Q\theta \quad (11)$$

$$\frac{\partial C}{\partial t}-\frac{\partial C}{\partial y}=\frac{1}{S_c}\frac{\partial^2C}{\partial y^2}+S_r\frac{\partial^2\theta}{\partial y^2}-K_rC \quad (12)$$

With initial and boundary conditions

$$\left.\begin{aligned}
&t\le 0; \quad u=0, \quad \theta=0, \quad C=0 \quad \forall y\\
&t>0; \quad u=1, \quad \theta=e^{-t}, \quad C=e^{-t} \quad at\ y=0\\
&u\to 0, \quad \theta\to 0, \quad C\to 0 \quad as\ \ y\to\infty
\end{aligned}\right\} \quad (13)$$

The degree of practical interest includes the Skin friction coefficients τ, local Nusselt Nu, and local Sherwood Sh numbers are given as follows:

$$\tau = -\left(1+\frac{1}{\beta}\right)\left(\frac{\partial u}{\partial y}\right)_{y=0}, \; N_u = -\left(\frac{\partial \theta}{\partial y}\right)_{y=0}, \; Sh = -\left(\frac{\partial C}{\partial y}\right)_{y=0} \tag{14}$$

III. NUMERICAL METHOD OF SOLUTION

Exact solution of system of partial differential Equations 10, 11 and 12 with boundary conditions given by Equation 13 are impossible. So, these equations we have solved by Crank-Nicolson implicit finite difference method. The Crank-Nicolson finite difference implicit method is a second order method in time ($o(\Delta t^2)$) and space, hence no restriction on space and time steps, that is, the method is unconditionally stable. The computation is executed for $\Delta y = 0.1$, $\Delta t = 0.001$ and procedure is repeated till $y = 4$. Equations 10, 11 and 12 are expressed as

$$\frac{u_{i,j+1}-u_{i,j}}{\Delta t}-\frac{u_{i+1,j}-u_{i,j}}{\Delta y}=\left(1+\frac{1}{\beta}\right)\frac{u_{i-1,j}-2u_{i,j}+u_{i+1,j}+u_{i-1,j+1}-2u_{i,j+1}+u_{i+1,j+1}}{2(\Delta y)^2}$$
$$+G_r\left(\frac{\theta_{i,j+1}+\theta_{i,j}}{2}\right)+G_m\left(\frac{C_{i,j+1}+C_{i,j}}{2}\right)-\left(M_1+\frac{1}{K}\right)\left(\frac{u_{i,j+1}+u_{i,j}}{2}\right) \tag{15}$$

$$\frac{\theta_{i,j+1}-\theta_{i,j}}{\Delta t}-\frac{\theta_{i+1,j}-\theta_{i,j}}{\Delta y}=\frac{1}{P_r}\left(1+\frac{4R}{3}\right)\left(\frac{\theta_{i-1,j}-2\theta_{i,j}+\theta_{i+1,j}+\theta_{i-1,j+1}-2\theta_{i,j+1}+\theta_{i+1,j+1}}{2(\Delta y)^2}\right)$$
$$+D_u\left(\frac{C_{i-1,j}-2C_{i,j}+C_{i+1,j}+C_{i-1,j+1}-2C_{i,j+1}+C_{i+1,j+1}}{2(\Delta y)^2}\right)+E_c\left(\frac{u_{i+1,j}-u_{i,j}}{\Delta y}\right)^2-Q\left(\frac{\theta_{i,j+1}+\theta_{i,j}}{2}\right) \tag{16}$$

$$\frac{C_{i,j+1}-C_{i,j}}{\Delta t}-\frac{C_{i+1,j}-C_{i,j}}{\Delta y}=\frac{1}{S_c}\left(\frac{C_{i-1,j}-2C_{i,j}+C_{i+1,j}+C_{i-1,j+1}-2C_{i,j+1}+C_{i+1,j+1}}{2(\Delta y)^2}\right) \tag{17}$$
$$+S_r\left(\frac{\theta_{i-1,j}-2\theta_{i,j}+\theta_{i+1,j}+\theta_{i-1,j+1}-2\theta_{i,j+1}+\theta_{i+1,j+1}}{2(\Delta y)^2}\right)+K_r\left(\frac{C_{i,j+1}+C_{i,j}}{2}\right)$$

Initial and boundary conditions are also rewritten as:

$$\begin{aligned} &u_{i,0}=0, \quad \theta_{i,0}=0, \quad C_{i,0}=0 && \forall i \\ &u_{0,j}=1, \quad \theta_{0,j}=e^{-j\Delta t}, \quad C_{0,j}=e^{-j\Delta t} && \forall j \\ &u_{l,j}\to 0, \quad \theta_{l,j}\to 0, \quad C_{l,j}\to 0 \end{aligned} \tag{18}$$

Where index i represents to y and j represents to time t, $\Delta t = tj+1-tj$ and $\Delta y = yi+1-yi$. Getting the values of u, θ and C at time t, we may compute the values at time $t+\Delta t$ as following method: we substitute i = 1, 2, ..., $l-1$, where n correspond to ∞ ,equations 15 to 17 give tridiagonal system of equations with boundary conditions in equation 18, are solved employing Thomas algorithm as discussed in Carnahan et al.[20], we find values of θ and C for all values of y at $t + \Delta t$. Equation 15 is solved by same to substitute these values of θ and C, we get solution for u till desired time t.

IV. ANALYSIS ON OBTAINED RESULTS

The present work analyzes the boundary layer unsteady MHD Casson flow past a porous vertical plate with the Soret-Dufour effect and Hall current. The influence of the order chemical reaction has been incorporated in the mass equation. In order to see a physical view of work, numerical results of velocity profile u, temperature profile θ, concentration profile C have been discussed with the help of graphs and skin friction coefficients, Nusselt number and Sherwood number are discussed with the help of tables. The following values are used for investigation Gr = 4.2, Gm = 6, K = 1.5, M_1= 0.2, β= 0.35, Kr = 1.4, Pr = 0.6, Du = 0.2, Sc = 0.25, Sr =1.7, R =1.8, Ec =2, Q =3, t = 0.1.

It is noted from figure 7 that increasing radiation parameter R, velocity u increases. This is correct observation because the increase in radiation reveals heat energy to flow. It is analyzed that an increase in R, temperature θ increases and it is notable that an increase in R, concentration C near to plate decrease after that increases in figure 25. In figure 6, velocity decreases as Prandtl number Pr increases and temperature decreases in figure 15 when Pr increases. In figure 21 concentration C near to plate increases and some distance from plate concentration decreases as Prandtl number increases. Figure 16 depicts the importance of radiation on temperature distribution. Figure 23, depicts the variation of Schmidt number Sc as concentration decreases rapidly with increase Sc while velocity profile in figure 9 decreases near to plate. In figure 1, 19 and 12, it is seen that velocity increases and concentration decreases as increase Dufour number Du, whereas temperature increases as Du increases. Figure 3 shows that increment in porosity parameter K results in an increase in velocity. Figures 8 and 22 depict the behavior of chemical reaction parameter Kr on velocity and concentration respectively. It is seen that velocity decreases, concentration decreases rapidly as Kr increase. The negative value of $Q < 0$ means heat absorption and the positive value of $Q > 0$ means heat transfer. In figure 4, velocity profile decreases on increasing heat source/sink parameter Q and also reducing momentum boundary layer. Figure 13 analyzed the impact of heat source/sink parameter Q in the temperature profile. It can be seen that the temperature profile decreases rapidly and the thermal boundary layer reduces for an increase of heat source parameter but it increases with the heat sink parameter. Figure 20, depicts that concentration profile increases near to plate from middle of boundary layer it decreases as well as species boundary layer reduces on an increase of heat source/sink parameter. Figure 11, 18 and 26 reveals that velocity, temperature and concentration increase on increase of time. Figure 14 described that increment in Ec results in temperature increases. In Figure 2, velocity near plate increases rapidly and then decreases rapidly. Figure 5 reveals that an increase in hall current parameter M_1 then velocity increases slowly. Figure 10, 24 and 17 depict that increment in Soret number Sr, velocity and concentration increases while temperature decreases respectively.

It is observed from *Table 1* that Change in Schmidt number Sc effects as skin friction coefficient and Sherwood number increases while Nusselt number decreases. Pr effects as skin friction coefficient and Sherwood number decrease while Nusselt number decreases. Skin friction coefficient and Sherwood number Sh increase whereas Nusselt number decreases with Dufour number Du increases and Eckert number Ec increases. Increase in Soret number Sr, Skin friction and Nusselt number Nu increase while Sherwood number Sh decreases. On increasing Casson fluid parameter β results in skin friction coefficient and Sherwood number Sh increases and Nusselt number decreases. On increasing Hall current parameter M_1 results in skin friction coefficient and Sherwood number Sh increases and Nusselt number decreases. It is also noted that increment in Q heat source/sink the skin friction coefficient and Sherwood number decrease while Nusselt number increases.

V. CONCLUSION

Effect of Hall current, viscous dissipation, first order chemical reaction, changes in Soret-Dufour effects on unsteady MHD flow past a vertical porous plate immersed in a porous medium are analyzed. This investigation the following conclusions have come:

5.1 It has been observed that on increasing Hall current parameter the velocity of the fluid increases.

5.2 The effect of radiation on concentration is noteworthy. It is observed that increasing values of R, concentration falls down and after some distance from the plate, it goes up slowly-slowly while velocity and temperature increases.

5.3 Interestingly, increment in concentration has been found on increasing Prandtl number P r.

5.4 For increasing values of Kr, it is a considerable enhancement in velocity, i.e. velocity decreases slowly but concentration decreases rapidly.

5.5 Increasing values of Dufour number, it is observed that velocity and temperature profile in the thermal boundary layer increases whereas concentration profile first decreases after then increases slowly in the boundary layer.

5.6 Schmidt number greatly influences the concentration profile in the concentration boundary layer.

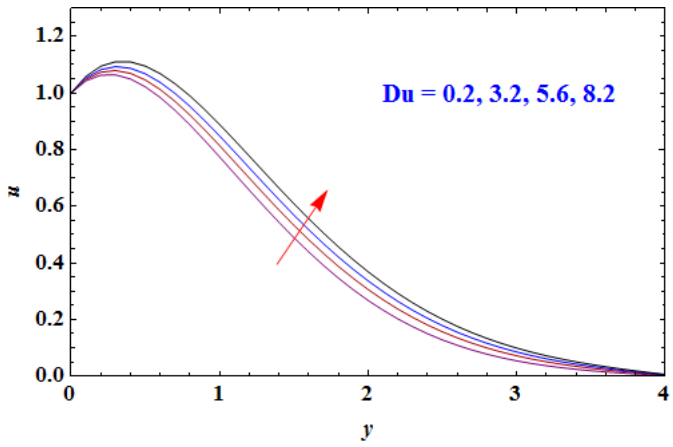

Fig. 1: Velocity Profiles for Different Values of Du

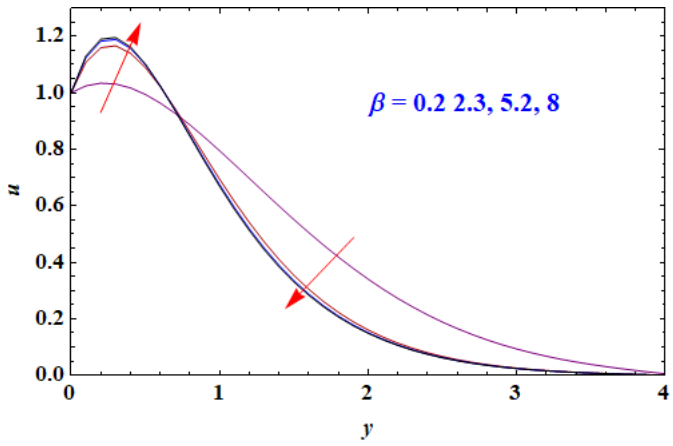

Fig. 2: Velocity Profiles for Different Values of β

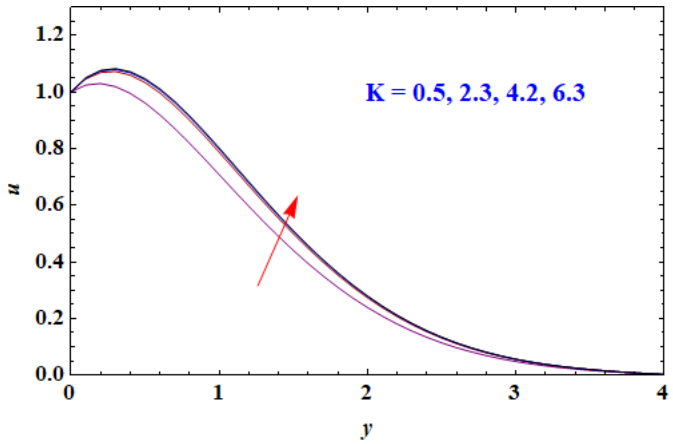

Fig. 3: Velocity Profiles for Different Valuesof K

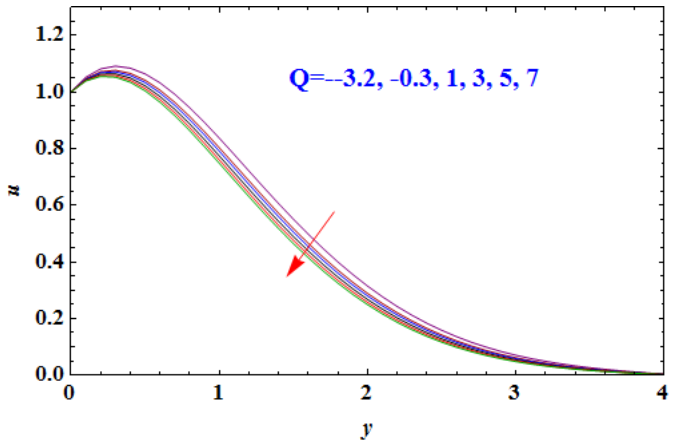

Fig. 4: Velocity Profiles for Different Values of Q

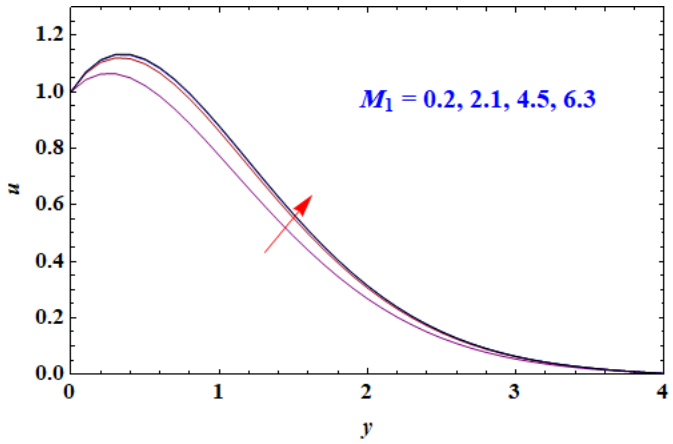

Fig. 5: Velocity Profiles for Different Values of M_1

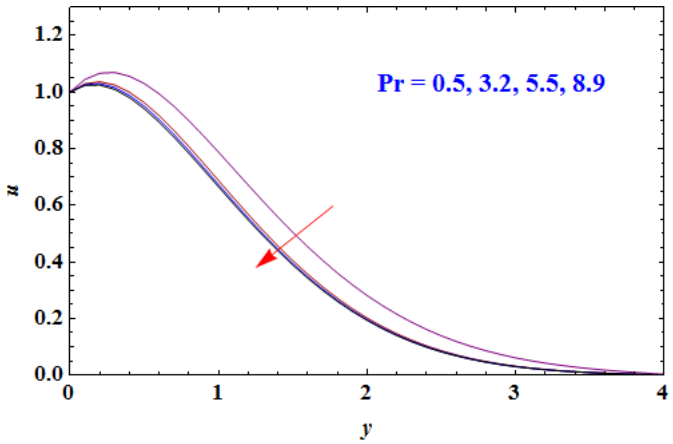

Fig. 6: Velocity Profiles for Different Values of Pr

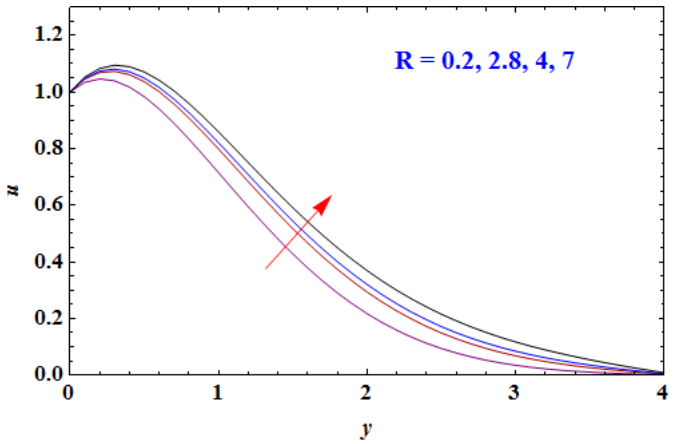

Fig. 7: Velocity Profiles for Different Values of R

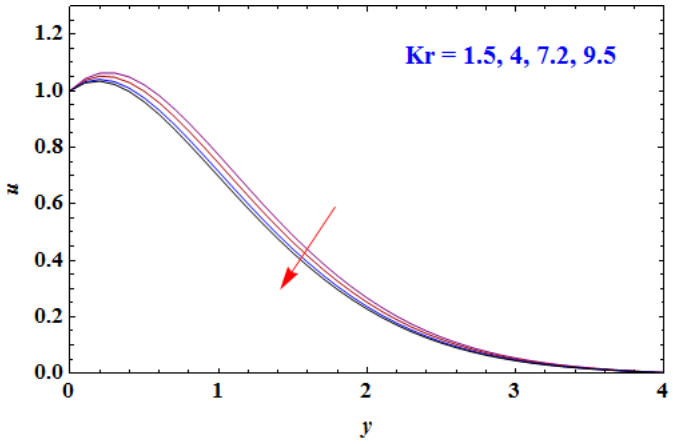

Fig. 8: Velocity Profiles for Different Values of Kr

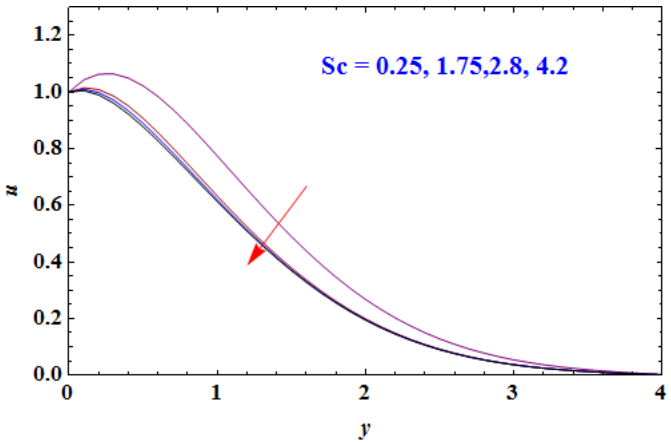

Fig. 9: Velocity Profiles for Different Values of Sc

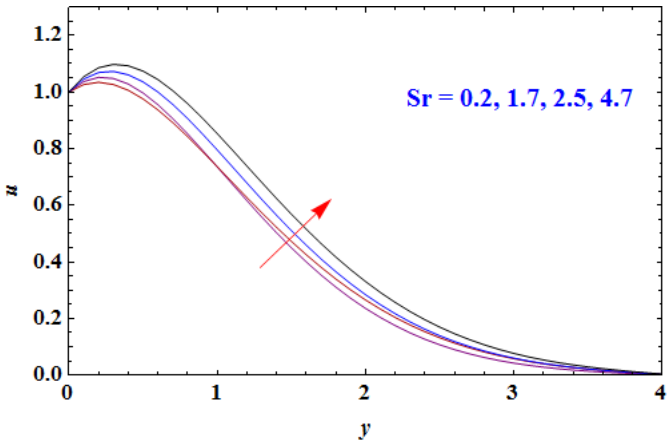

Fig. 10: Velocity Profiles for Different Values of Sr

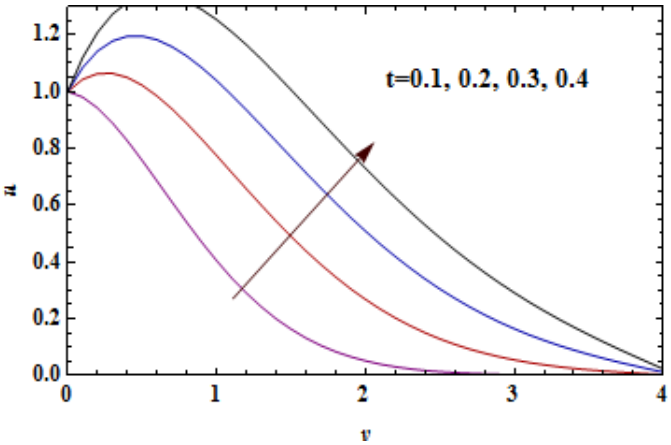

Fig. 11: Velocity Profiles for Different Values of t

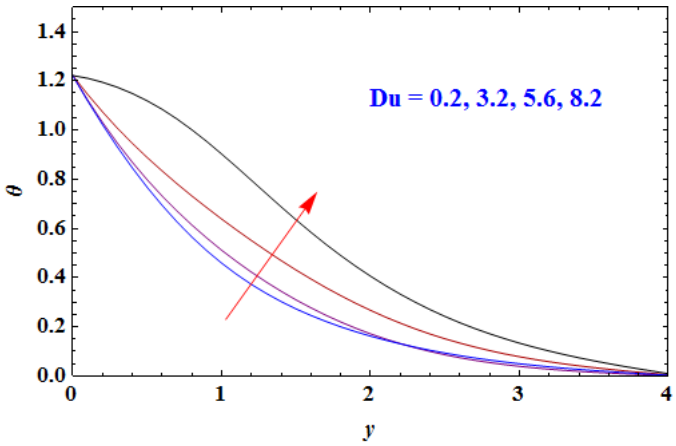

Fig. 12: Temperature Profiles for Different Values of Du

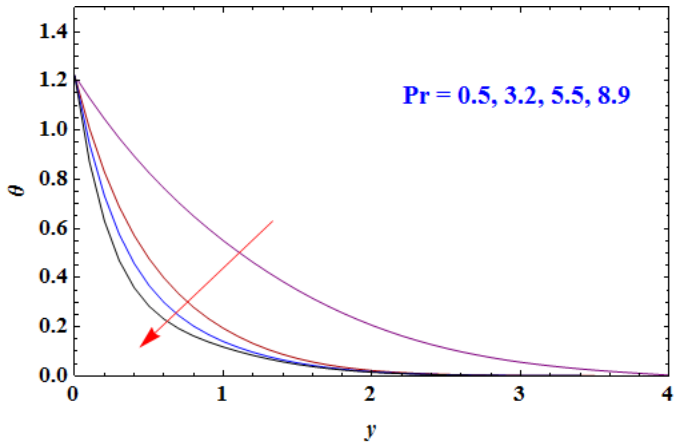

Fig. 15: Temperature Profiles for Different Values of Pr

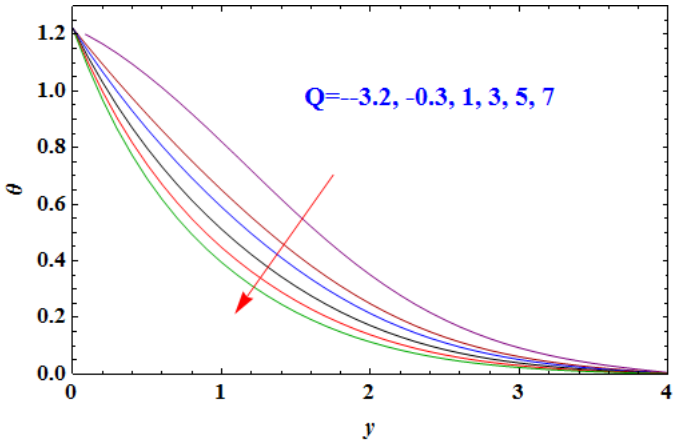

Fig. 13: Temperature Profiles for Different Values of Q

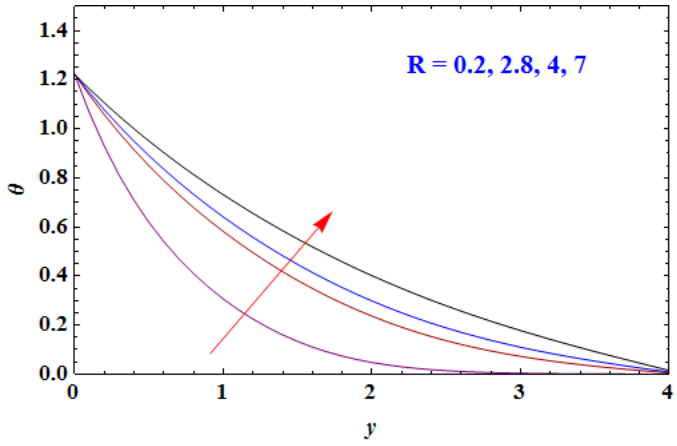

Fig. 16: Temperature Profiles for Different Values of R

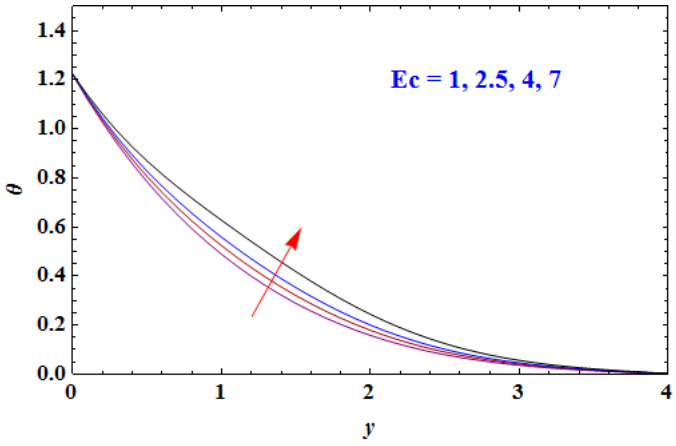

Fig. 14: Temperature Profiles for Different Values of Ec

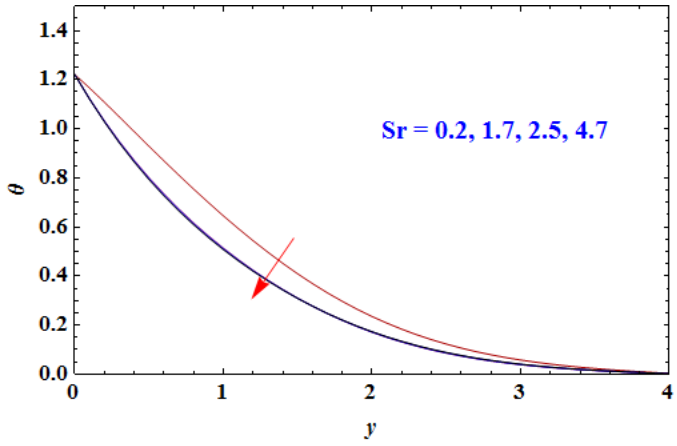

Fig. 17: Temperature Profiles for Different Values of Sr

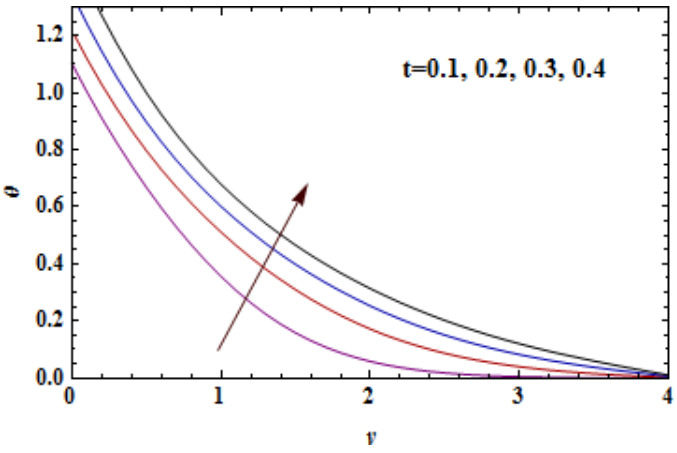

Fig. 18: Temperature Profiles for Different Values of t

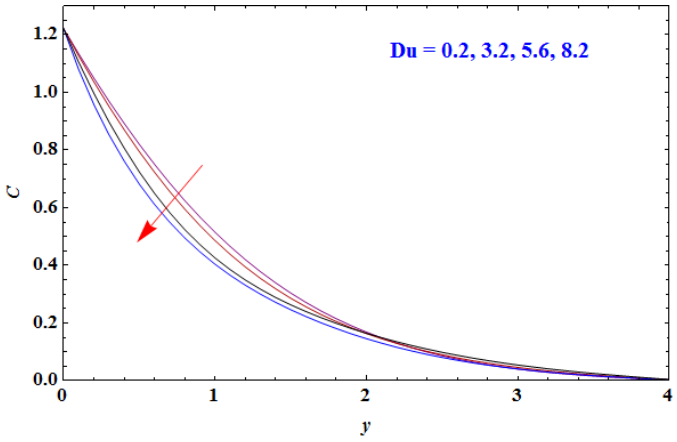

Fig. 19: Concentration Profiles for Different Values of Du

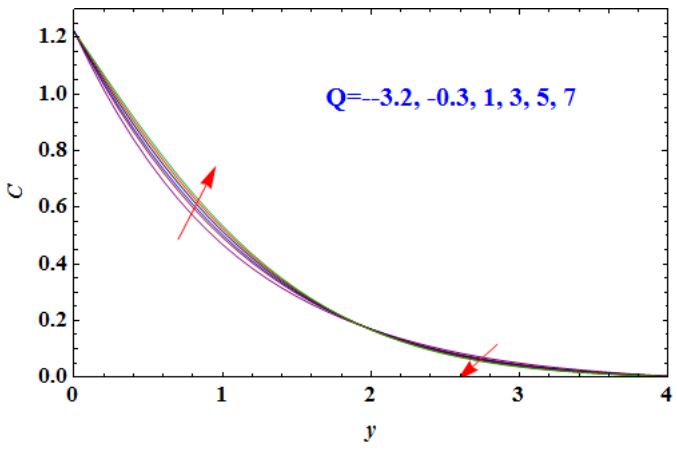

Fig. 20: Concentration Profiles for Different Values of Q

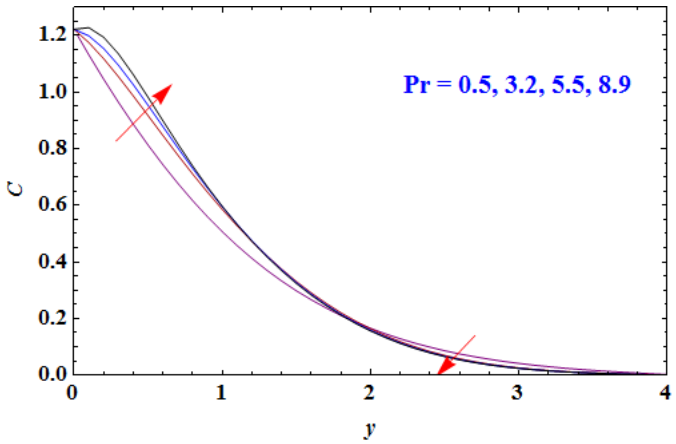

Fig. 21: Concentration Profiles for Different Values of Pr

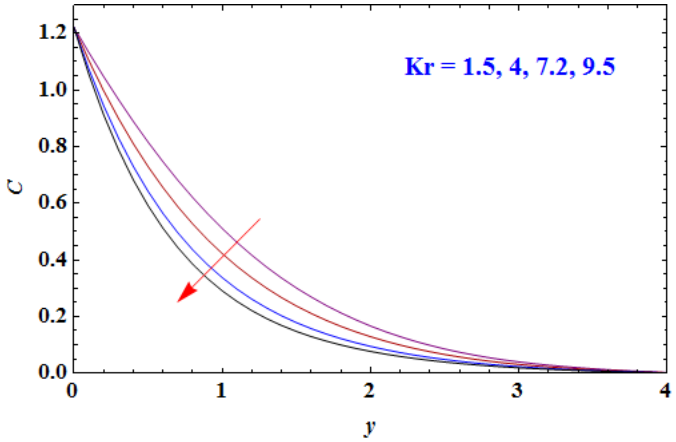

Fig. 22: Concentration Profiles for Different Values of Kr

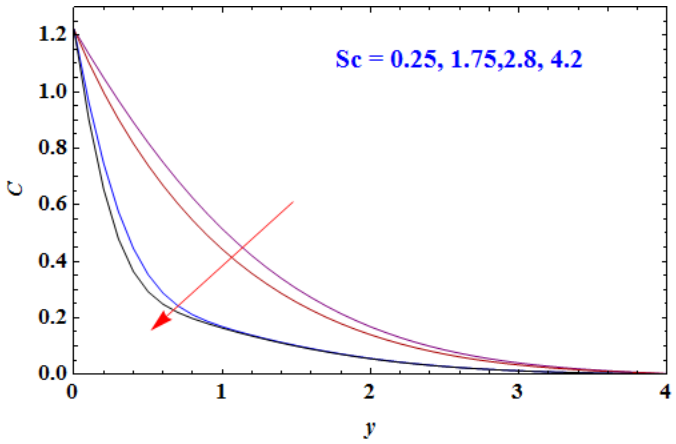

Fig. 23: Concentration Profiles for Different Values of Sc

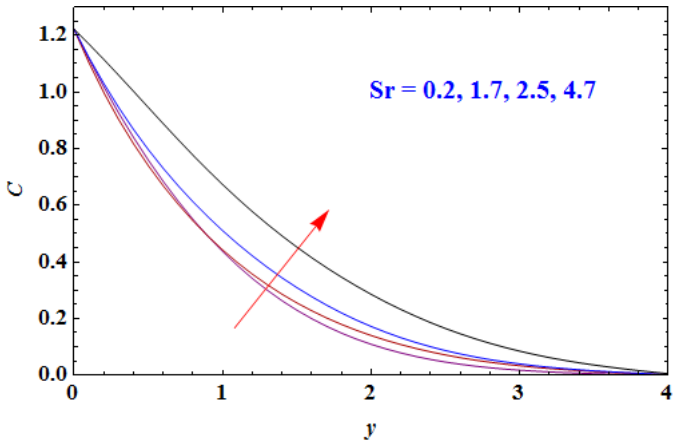

Fig. 24: Concentration Profiles for Different Values of Sr

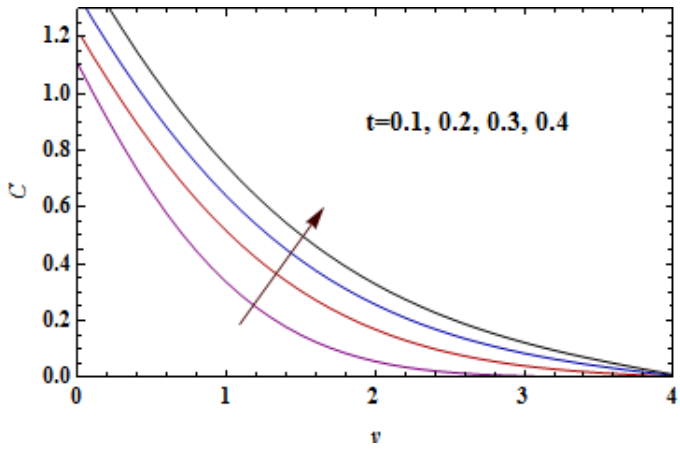

Fig. 26:Concentration Profiles for Different Values of t

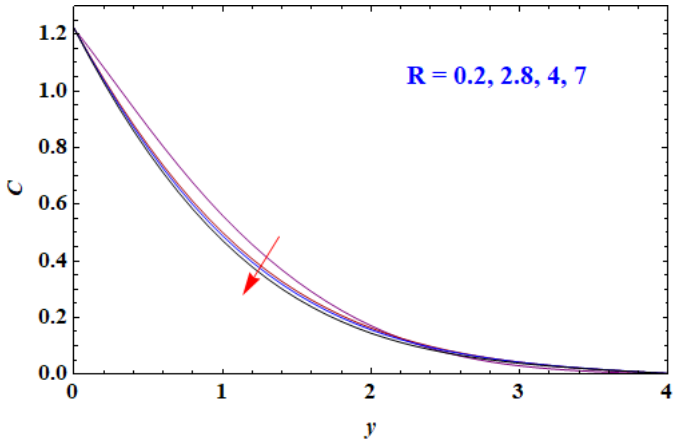

Fig. 25: Concentration Profiles for Different Values of R

Table 1. Skin friction coefficient τ, Nusselt number Nu and Sherwood number Sh for different values of parameters taking fix values of Gr = 4.2, Gm = 6, K = 1.5, M_1= 0.2, β= 0.2, Kr = 1.4, Pr = 0.6, Du = 0.2, Sc = 0.25, Sr =1.7, R =1.8, Ec =2, Q =3, t = 0.1.

β	Du	Ec	K	Kr	Pr	R	M_1	S_c	Sr	Q	t	τ	Nu	Sh
0.2	0.2	2	1.5	1.4	0.6	1.8	0.2	0.25	1.7	3	0.1	1.47062	1.0054	0.873165
2.3	0.2	2	1.5	1.4	0.6	1.8	0.2	0.25	1.7	3	0.1	1.55363	0.948078	0.889804
5.2	0.2	2	1.5	1.4	0.6	1.8	0.2	0.25	1.7	3	0.1	1.48919	0.937503	0.892974
8	0.2	2	1.5	1.4	0.6	1.8	0.2	0.25	1.7	3	0.1	1.46724	0.93406	0.894012
0.35	**0.2**	2	1.5	1.4	0.6	1.8	0.2	0.25	1.7	3	0.1	1.65241	0.992201	0.876917
0.35	**3.2**	2	1.5	1.4	0.6	1.8	0.2	0.25	1.7	3	0.1	1.85239	0.764003	0.947336
0.35	**5.6**	2	1.5	1.4	0.6	1.8	0.2	0.25	1.7	3	0.1	2.03522	0.514929	1.02852
0.35	**8.2**	2	1.5	1.4	0.6	1.8	0.2	0.25	1.7	3	0.1	2.26875	0.109025	1.16889
0.35	0.2	**1**	1.5	1.4	0.6	1.8	0.2	0.25	1.7	3	0.1	1.62226	1.02237	0.868285
0.35	0.2	**2.5**	1.5	1.4	0.6	1.8	0.2	0.25	1.7	3	0.1	1.66744	0.977248	0.881188
0.35	0.2	**4**	1.5	1.4	0.6	1.8	0.2	0.25	1.7	3	0.1	1.71233	0.932884	0.89383
0.35	0.2	**7**	1.5	1.4	0.6	1.8	0.2	0.25	1.7	3	0.1	1.80132	0.846208	0.918412
0.35	0.2	2	**0.5**	1.4	0.6	1.8	0.2	0.25	1.7	3	0.1	0.950611	0.992346	0.877565

0.35	0.2	2	**2.3**	1.4	0.6	1.8	0.2	0.25	1.7	3	0.1	1.78111	0.991901	0.876891
0.35	0.2	2	**4.2**	1.4	0.6	1.8	0.2	0.25	1.7	3	0.1	1.89192	0.991573	0.876892
0.35	0.2	2	**6.3**	1.4	0.6	1.8	0.2	0.25	1.7	3	0.1	1.93707	0.99142	0.876899
0.35	0.2	2	1.5	**1.8**	0.6	1.8	0.2	0.25	1.7	3	0.1	1.64311	0.991866	0.889224
0.35	0.2	2	1.5	**4**	0.6	1.8	0.2	0.25	1.7	3	0.1	1.43161	0.983849	1.17117
0.35	0.2	2	1.5	**7.2**	0.6	1.8	0.2	0.25	1.7	3	0.1	1.21004	0.974585	1.47333
0.35	0.2	2	1.5	**9.5**	0.6	1.8	0.2	0.25	1.7	3	0.1	1.07724	0.968551	1.65972
0.35	0.2	2	1.5	1.4	**0.5**	1.8	0.2	0.25	1.7	3	0.1	1.71762	0.911549	0.901144
0.35	0.2	2	1.5	1.4	**3.2**	1.8	0.2	0.25	1.7	3	0.1	1.1256	2.15668	0.470401
0.35	0.2	2	1.5	1.4	**5.5**	1.8	0.2	0.25	1.7	3	0.1	0.993012	2.78179	0.229897
0.35	0.2	2	1.5	1.4	**8.9**	1.8	0.2	0.25	1.7	3	0.1	0.891104	3.51046	-0.059222
0.35	0.2	2	1.5	1.4	0.6	**0.2**	0.2	0.25	1.7	3	0.1	1.32212	1.56809	0.685784
0.35	0.2	2	1.5	1.4	0.6	**2.8**	0.2	0.25	1.7	3	0.1	1.77127	0.850637	0.918876
0.35	0.2	2	1.5	1.4	0.6	**4**	0.2	0.25	1.7	3	0.1	1.87712	0.742687	0.948992
0.35	0.2	2	1.5	1.4	0.6	**7**	0.2	0.25	1.7	3	0.1	2.05248	0.593058	0.988149
0.35	0.2	2	1.5	1.4	0.6	1.8	**0.2**	0.25	1.7	3	0.1	1.65241	0.992201	0.876917
0.35	0.2	2	1.5	1.4	0.6	1.8	**2.1**	0.25	1.7	3	0.1	2.51597	0.988477	0.87732
0.35	0.2	2	1.5	1.4	0.6	1.8	**4.5**	0.25	1.7	3	0.1	2.67912	0.987309	0.877551
0.35	0.2	2	1.5	1.4	0.6	1.8	**6.3**	0.25	1.7	3	0.1	2.70604	0.987102	0.877594
0.35	0.2	2	1.5	1.4	0.6	1.8	0.2	**0.25**	1.7	3	0.1	1.65241	0.992201	0.876917
0.35	0.2	2	1.5	1.4	0.6	1.8	0.2	**1.75**	1.7	3	0.1	0.579633	0.95069	2.06938
0.35	0.2	2	1.5	1.4	0.6	1.8	0.2	**2.8**	1.7	3	0.1	0.360793	0.933651	2.58939
0.35	0.2	2	1.5	1.4	0.6	1.8	0.2	**4.2**	1.7	3	0.1	0.18523	0.913773	3.18956
0.35	0.2	2	1.5	1.4	0.6	1.8	0.2	0.25	**0.2**	3	0.1	1.43314	0.985206	1.04842
0.35	0.2	2	1.5	1.4	0.6	1.8	0.2	0.25	**1.7**	3	0.1	1.65241	0.992201	0.876917
0.35	0.2	2	1.5	1.4	0.6	1.8	0.2	0.25	**2.5**	3	0.1	1.77073	0.995712	0.783784
0.35	0.2	2	1.5	1.4	0.6	1.8	0.2	0.25	**4.7**	3	0.1	2.10084	1.00453	0.522318
0.35	0.2	2	1.5	1.4	0.6	1.8	0.2	0.25	1.7	**-3.2**	0.1	-2.01681	0.251471	1.07677
0.35	0.2	2	1.5	1.4	0.6	1.8	0.2	0.25	1.7	**-0.3**	0.1	-1.82303	0.638556	0.976345
0.35	0.2	2	1.5	1.4	0.6	1.8	0.2	0.25	1.7	**1**	0.1	-1.7504	0.787159	0.93551
0.35	0.2	2	1.5	1.4	0.6	1.8	0.2	0.25	1.7	**3**	0.1	-1.65241	0.992201	0.876917
0.35	0.2	2	1.5	1.4	0.6	1.8	0.2	0.25	1.7	**5**	0.1	-1.56829	1.17375	0.822771
0.35	0.2	2	1.5	1.4	0.6	1.8	0.2	0.25	1.7	**7**	0.1	-1.49549	1.33633	0.772438
0.35	0.2	2	1.5	1.4	0.6	1.8	0.2	0.25	1.7	3	**0.1**	-0.759763	0.993876	1.00151
0.35	0.2	2	1.5	1.4	0.6	1.8	0.2	0.25	1.7	3	**0.2**	1.65241	0.992201	0.876917
0.35	0.2	2	1.5	1.4	0.6	1.8	0.2	0.25	1.7	3	**0.3**	3.25035	1.0526	0.883938
0.35	0.2	2	1.5	1.4	0.6	1.8	0.2	0.25	1.7	3	**0.4**	4.59795	1.12637	0.938618

ACKNOWLEDGEMENT

We acknowledge our principal Dr. V. C. Tripathi and chief proctor of science faculty Dr A. K. Dwivedi and thank for encouraging to complete this research work.

REFERENCES

[1] Shafiq A., Rasool G. and Tlili I. (2020), "Marangoni convective nanofluid flow over an electromagnetic actuator in the presence of first-order chemical reaction" Heat Transf. Asian Res /Vol.49/ Pp. 274–288.

[2] Parvin S.; Mohamed Isa S.S.P., Arifin, N.M., Md Ali, F. (2021), "The Inclined Factors of Magnetic Field and Shrinking Sheet in Casson Fluid Flow, Heat and Mass Transfer Symmetry"/Vol.13/ No.373, https://doi.org/10.3390/sym13030373.

[3] Lahmar Sihem, Kezzar Mohamed, Eid Mohamed R., and Sari, Mohamed Rafik (2020), "Heat transfer of squeezing unsteady nanofluid flow under the effects of an inclined magnetic field and variable thermal conductivity" Physica A: Statistical Mechanics and its Applications, Elsevier / Vol. 540(C).

[4] M. R. Eid, K. Mahny, A. Dar and T. Muhammad (2020), "Numerical study for Carreau nanofluid flow over aconvectively heated nonlinear stretching surface with chemically reactive species" Physica A: Statistical Mechanics and Its Applications /Vol. 540/ 123063.

[5] Hammad Alotaibi, Saeed Althubiti, Mohamed R. Eid, K. L. Mahny (2021), "Numerical Treatment of MHD Flow of

Casson Nanofluid via Convectively Heated Non-Linear Extending Surface with Viscous Dissipation and Suction/Injection Effects" /Vol. 66/ No.1, Pp. 229-245, doi:10.32604/cmc.2020.012234.

[6] K. K. Asogwa and A. A. Ibe, (2020), "A Study of MHD Casson Fluid Flow over a Permeable Stretching Sheet with Heat and Mass Transfer" Journal of Engineering Research and Reports /Vol. 16/ No.2, Pp. 10-25.

[7] Renu Devi, Vikas Poply, Manimala (2021), "Effect of aligned magnetic field and inclined outer velocity in casson fluid flow over a stretching sheet with heat source" Journal of Thermal Engineering /Vol.7/ No.4, Pp. 823-844.

[8] K Kumar Anantha, , Ankalagiri Ramudu Sugunamma Vangala, Dr.N. Sandeep (2021), "Impact of Soret and Dufour on MHD Casson fluid flow past a stretching surface with convective-diffusive conditions" Journal of Thermal Analysis and Calorimetry 10.1007/s10973-021-10569-w.

[9] U. S. Mahabaleshwar, K. N. Sneha, Akio Miyara, M. Hatami (2022), "Radiation effect on inclined MHD flow past a super-linear stretching/shrinking sheet including CNTs, Waves in Random and Complex Media" DOI: 10.1080/17455030.2022.2053238.

[10] Ram Prakash Sharma and Sachin Shaw (2022), "MHD Non-Newtonian Fluid Flow past a Stretching Sheet under the Influence of Non-linear Radiation and Viscous Dissipation" J. Appl. Comput. Mech. /Vol. 8/ No. 3, Pp. 949-961.

[11] Naveed Akbar, Sardar Muhammad Hussain and Riaz Ullah Khan (2022), "Numerical Solution of Casson Fluid Flow under Viscous Dissipation and Radiation Phenomenon" Journal of Applied Mathematics and Physics /Vol. 10/ Pp. 475-490.

[12] Elham Alali Elham Alali and Ahmed M. Megahed (2022), "MHD dissipative Casson nanofluid liquid film flow due to an unsteady stretching sheet with radiation influence and slip velocity phenomenon" Nanotechnology Reviews/ Vol. 11/ Pp. 463–472

[13] T. M. Ajayi, A. J. Omowaye, and I. L. Animasaun(2017), "Viscous Dissipation Effects on the Motion of Casson Fluid over an Upper Horizontal Thermally Stratified Melting Surface of a Paraboloid of Revolution: Boundary Layer Analysis" Hindawi Journal of Applied Mathematics /Vol. 2017/ https://doi.org/10.1155/2017/1697135.

[14] N. Pandya and A. K. Shukla (2014), "Effects of Thermophoresis, Dufour, Hall and Radiation on an Unsteady MHD flow past an Inclined Plate with Viscous Dissipation" International Journal of Mathematics and Scientific Computing /Vol. 4/ No. 2.

[15] Mallikarjuna B, Ramprasad S and Chakravarthy YSK. Multiple slip and inspiration effects on hydromagnetic Casson fluid in a channel with stretchable walls. Int J Heat Technol 2020; 38: 817–826.

[16] Bukhari Z, Ali A, Abbas Z, et al. The pulsatile flow of thermally developed non-Newtonian Casson fluid in a channel with constricted walls. AIP Adv 2021; 11: 025324.

[17] Divya BB, Manjunatha G, Rajashekhar C, et al. Analysis of temperature dependent properties of a peristaltic MHD flow in a non-uniform channel: a Casson fluid model. Ain Shams Eng J 2021; 12: 2181–2191.

[18] Ahmad Sheikh N, Ling Chuan Ching D, Abdeljawad T, et al. A fractal-fractional model for the MHD flow of Casson fluid in a channel. Comput Mater Contin 2021; 67: 1385–1398.

[19] Haroon Ur Rasheed, Saeed Islam, Zeeshan, Waris Khan, Jahangir Khan and Tariq Abbas, Numerical modeling of unsteady MHD flow of Casson fluid in a vertical surface with chemical reaction and Hall current, Advances in Mechanical Engineering 2022, Vol. 14(3) 1–10

[20] Brice Carnahan, H.A. Luther and James O. Wilkes. (1990), Applied Numerical Methods, Krieger Pub Co, Florida.

[21] T. G. Cowling (1990), Magneto-Hydrodynamics, Inter Science Publishers, New York.